Hydrothermal Synthesis of Zirconia/Silica Hybrid Materials and their Application on Cotton Fabrics

Ming-Shien Yen*

Department of Materials Engineering, Kun Shan University, Tainan 71003, Taiwan

Abstract *— A series of novel zirconia/silica hybrid materials were prepared via the hydrothermal process from zirconium n-propoxide (ZNP), tetraethoxysilane (TEOS), and n-octyltriethoxysilane (OTES). The structures of the zirconia/silica hybrid materials were characterized using Fourier transform infrared (FTIR) analysis and ^{29}Si nuclear magnetic resonance (NMR) imaging. Grey cotton fabrics were first dyed and then coated with the zirconia/silica hybrid materials through a padding–drying–thermosol process. The bonding structures of the treated cotton fabrics were evaluated using scanning electron microscopy (SEM) and energy dispersive X-ray spectroscopy (EDS) analyses. The evenness of the coated layer on the treated cotton fabrics was confirmed by SEM images, and the interaction of the hybrid materials with the treated cotton fabrics was verified. Moreover, water repellency and warmth retention analyses of the treated fabrics were conducted. Our data show that the warmth retention of the cotton fabrics treated with the zirconia/silica hybrid materials was improved with increasing concentrations of zirconium n-propoxide in the reaction mixture. After modification with zirconia/silica hybrid materials, all the treated cotton fabrics revealed good water repellency abilities.*

Keywords *— zirconia, silicacotton fabrics, hydrothermal, warmth retention, water repellency.*

I. INTRODUCTION

Most new products are designed to have multiple functions and a form of intelligence. Thus, hybrid materials have recently become one of the main trends in materials science research. Compared to traditional materials, the most important feature of a hybrid material is its designability. The mechanical, physical, and chemical properties of a hybrid material can be designed and controlled by changing its composition or using interface control, compounding technology, or molding technology to meet the requirements of maximum usability and environmental compatibility [1–3]. Organic–inorganic hybrid materials contain both organic and inorganic functionalities and provide functional compensation and optimization [4–8]. Consequently, they are widely used in numerous fields including optics, catalysis, and in other biomaterials.

Zirconia (ZrO_2) is an interesting oxide material that has been developed recently. Zirconia offers ablation resistance, chemical stability, and a high refractive index; it also possesses good dielectric, insulating, and mechanical properties [9-12]. It is applied in thermal-barrier-, bioactive-, ultrafiltration-, and corrosion-protection coatings [13-17], as well as during the manufacture of photoelectric components and electrochemical biosensors [18-21]. It is frequently used in various industries, including aviation, aerospace, ferrous metallurgy, machine manufacture, and optics. In addition, it offers strong potential for other applications. There are many methods used to prepare the coating material; these methods can be classified into two major types, namely physical processes, such as vapor-deposition and sputtering methods, and chemical processes, such as chemical-vapor deposition, spray pyrolysis, and sol-gel methods. The sol–gel method is considered extremely practical for the fabrication of mesoporous ceramic membranes [22, 23].

Furthermore, silica is a natural material derived from common materials such as quartz, sand, and flint. It has high chemical stability, a low thermal expansion coefficient, and high heat-resistance characteristics. The relatively high chemical stability of the silica phase can be advantageous in some cases [24-27]. Khatib's use of silica membranes for a hydrogen separation application reveals that silica-based membranes have emerged as promising materials at high temperatures owing to their high permeation rates, high selectivity, hydrothermal stability, resistance to poisons, and mechanical strength [28].

Hydrothermal method provides advantages such as direct crystallization under hydrothermal conditions without sintering, regular morphology, uniform grain size, lower agglomeration, etc., it is widely used for the preparation of nanoparticles. It is also used in the preparation of hybrid materials that possess both the flexible performance of organic materials and the anti-friction, resistance to aging, and weathering characteristics of inorganic materials [29-32]. The

modification of inorganic–organic materials greatly improves the surface properties of the organic material and expands its application [33-36].

This study adopted the hydrothermal method to synthesize a series of composite materials of zirconium n-propoxide sol hybrids, with tetraethoxysilane (TEOS) and n-octyltriethoxysilane (OTES) as chemical precursors. Various molar ratios of the zirconia/silica hybrid materials were used to generate the network structures, and the chemical and physical properties of the treated cotton fabrics were evaluated. Water repellence and warmth retention were analyzed to evaluate the physical properties of the treated cotton fabrics and to identify multifunctional benefits.

II. EXPERIMENT

A. Materials

Milled, scoured, and bleached plain weave Cotton fabrics [ends (100)*picks (56)/(32s/1)*(32s/1)] were supplied by Everest Textile Industry Co., Ltd., Tainan, Taiwan. tetraethoxysilane, zirconium n-propoxide, and OTES were purchased from Acros Co., Ltd., Geel, Belgium. Sodium sulfate and sodium carbonate were purchased from Hayashi Pure Chemical Co., Ltd., Osaka, Japan. The reactive dye (C. I. reactive blue 19) was supplied by Everlight Chemical Industrial Co., Ltd., Taipei, Taiwan. The scouring agent laundry detergent (Lipofol TM-1000E) was supplied by Taiwan Nicca Chemical Industrial Co., Ltd., Taipei, Taiwan.

B. Preparation and processing

a) Dyeing of Cotton fabrics

Cotton fabrics were dyed using an infrared dyeing machine (LABTEC IRD-16) at a liquor ratio of 1:40 with distilled water. The dyeing bath was prepared with a reactive dye concentration of 2% on mass of fiber (o.m.f.), 20 g/L of sodium sulfate, and 10 g/L of sodium carbonate. Dyeing began at 30°C for 10 min, and then the dye bath temperature was increased at a rate of 2°C/min to 60°C and maintained at this temperature for 40 min, followed by cooling to 40°C. After dyeing, the fabrics were placed in a 2 g/L scouring agent liquor at 80°C for 20 minutes for two washings and then dried at room temperature.

b) Preparation of hybrid materials

For the zirconia synthesis, the zirconia sol solution derived from zirconium n-propoxide. We prepared zirconia gel by dissolving ZNP and ethanol using a 1:30 molar ratio; the ZNP was hydrolyzed in water using a 1:4 molar ratio. The mixture was heated under reflux for 30 min until it completely dissolved; the pH value was adjusted to approximately 3–4 using nitric acid, and the mixture was then stirred until it became clear. Then, constant ratios of TEOS and OTES were respectively prepared with 50 mL of deionized water and 5 mL of 99% ethanol. To complete the silica solution, the pH of the mixture was adjusted to 3.5 by adding 2 N hydrochloric acid at 40°C with vigorous stirring for 30 min. Hybrid materials $\mathbf{T_1}$–$\mathbf{T_4}$ were synthesized using ZNP:TEOS:OTES molar ratios of 2:4:0.5, 2:4:1, 2:4:2, and 2:4:3 (i.e., varying OTES amounts) in clave hydrothermal instrument for 8 h. Hybrid materials $\mathbf{Z_1}$–$\mathbf{Z_4}$ were synthesized using ZNP:TEOS:OTES molar ratios of 1:4:2, 2:4:2, 3:4:2 and 4:4:2 (i.e., varying ZNP amounts) in clave hydrothermal instrument for 8 h. The compositions of hybrid materials $\mathbf{T_1}$–$\mathbf{T_4}$ and $\mathbf{Z_1}$–$\mathbf{Z_4}$ are given in Table 1.

c) Treating Cotton fabrics

The treatment of the cotton fabrics was performed using the "two dips, two nips" padding method with a pickup of 80%. A were dipped for 3 min in a sol solution containing the required

Table 1. Composition of $\mathbf{T_1}$–$\mathbf{T_4}$ and $\mathbf{Z_1}$–$\mathbf{Z_4}$

Compd.	ZNP/TEOS/OTES	Compd.	ZNP/TEOS/OTES
$\mathbf{T_1}$	2:4:0.5	$\mathbf{P_1}$	1:4:2
$\mathbf{T_2}$	2:4:1	$\mathbf{P_2}$	2:4:2
$\mathbf{T_3}$	2:4:2	$\mathbf{P_3}$	3:4:2
$\mathbf{T_4}$	2:4:3	$\mathbf{P_4}$	4:4:2

weight percent of hybrid materials. A padding–drying–curing finishing procedure was used to disaggregate the agglomerated particles into well-dispersed colloidal particles. Fumed zirconia and silica sol-treated fabric samples were padded and nipped to remove excess liquid and to obtain a percent wet pickup of 80% using a padder (Rapid Labortex Co., Ltd., Taoyuan, Taiwan) with a set nipping pressure. The treated fabric was pre-dried in an oven at 70°C for 5 min. Then, the treated fabrics were cured at 100°C for 90 s in a preheated curing oven (R3, Chang Yang Machinery Co., Taiwan). The treated fabrics were rinsed with water several times to thoroughly remove any hybrid material residue and dried at 70°C for 5 min prior to analysis. The labels $\mathbf{CT_1}$–$\mathbf{CT_4}$ and $\mathbf{CZ_1}$–$\mathbf{CZ_4}$ denote the dyed cotton fabrics treated with hybrid materials $\mathbf{T_1}$–$\mathbf{T_4}$ and $\mathbf{Z_1}$–$\mathbf{Z_4}$, respectively. Figure 1 shows a schematic describing the interaction between the hybrid materials and fabric.

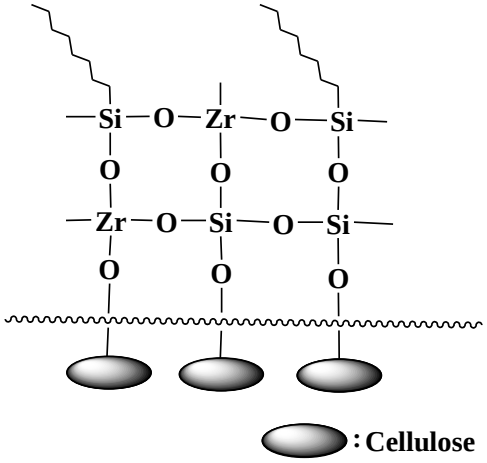

Fig. 1 Schematic describing the interaction between hybrid materials and fabrics.

III. RESULTS AND DISCUSSION

A. FTIR analysis

In the IR spectra of the **Z_1–Z_4** and **T_1–T_4** hybrid materials, a strong absorption band in the range from 3456 to 3444 cm^{-1} and 3452 to 3441 cm^{-1}, respectively, showed that the hybrid materials had N–H groups. Absorption peaks at approximately 451–447 cm^{-1} and 459–455 cm^{-1}, respectively, revealed that the hybrid materials had Zr–O groups, which enabled the formation of Zr–O–Zr networks. A second typical absorption region for the Si–O stretching vibration of **Z_1–Z_4** and **T_1–T_4** at 1072–1068 cm^{-1} and 1072–1070 cm^{-1}, respectively, has been reported. In the absorption region at 1188–1184 cm^{-1}, a band due to Si–C bond stretching was found, and the absorption region at 798–794 cm^{-1} was due to deformation of the Si–C bond. Asymmetric stretching vibrations of the C–H bonds in **Z_1–Z_4** and **T_1–T_4** were found from 2927 to 2925 cm^{-1} and from 2928 to 2927 cm^{-1}, respectively. Symmetric stretching vibrations of the C–H bonds of **Z_1–Z_4** and **T_1–T_4** were found from 2858 to 2854 cm^{-1} and from 2858 to 2856 cm^{-1}, respectively. Thus, it is reasonable to assume that reactions occurred between some of the zirconia and silica. Figure 2 shows the FTIR spectra of **Z_1–Z_4**. Increasing the zirconia concentration increased the strength of the Zr–O absorption and also strengthened the bonding. Figure 3 shows the FTIR spectra of **T_1–T_4**. Increasing the OTES concentration increased the strength of the Si–O absorption and strengthened the bonding. The structures of Si–O–Si and Zr–O–Zr were also analyzed using ^{29}Si NMR.

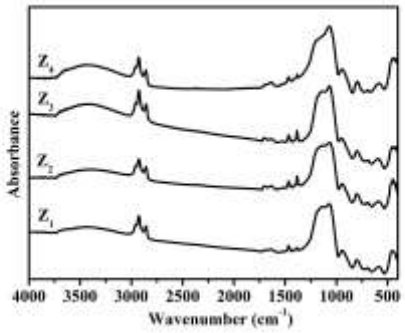

Fig. 2 FTIR spectra of hybrid materials **Z_1–Z_4**.

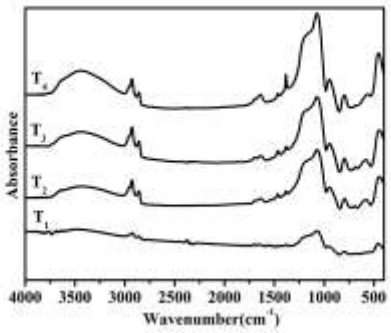

Fig. 3 FTIR spectra of hybrid materials **T_1–T_4**.

B. ^{29}Si NMR spectra analysis

^{29}Si NMR was used to observe the structure formed by the hydrolysis of Si. While the FTIR results indicate the formation of Si–O–Si by a hydrothermal reaction, ^{29}Si solid-state NMR provides data on the structure of the silica and the extent of the Si–OH condensation reaction. The ^{29}Si NMR spectra of **T_1–T_4**, shown in Figure 4, indicated that the increase in the molar ratio of OTES under constant molar amounts of ZNP and TEOS made the hybrid materials react more completely, so that the absorption peaks of hybrid materials tend to be smooth, and so the main absorption peaks of the hybrid materials **T_1–T_4** tend to be strong. The high-resolution solid-state NMR spectra of **T_1–T_4**, respectively, illustrated absorption peaks at T^2, corresponding to Si–OR, following the hydrolysis of TEOS with OTES, indicating that the absorption structure tended to be of the type (R–O)Si(–OSi≡)$_3$. The structure of the Si–OR absorption peak indicated that some Si quadruple bonds had an unreacted Si–OH functional group, (H–O)Si(–OSi≡)$_3$ and some Q^3 quadruple bonds had an unreacted Si–O functional group, Si(–OSi≡)$_3$. The structure of Q^4 indicates that the Si quadruple bond reacted completely with the Si–O functional group: Si(-OSi≡)$_4$. In the spectrum of hybrid **T_1** and **T_2**, the strength of the Q^3 absorption peak (at approximately -100.42 and -100.40 ppm) increased, and the Q^4 absorption peak appeared at a δ value of ~108.14 and -109.09 ppm. In addition, the weak absorption peak T^2 appeared at approximately −63.91 and −63.83 ppm. The results for hybrid **T_3**

indicated a Q^3 absorption peak at a δ value of ~100.06 ppm; the Q^4 absorption peak decreased, and the T^2 absorption peak increased significantly. Regarding hybrid **T_4**, the Q^3 absorption intensity increased substantially, and the T^2 absorption intensity increased. The Q^4 absorption peak for hybrids **T_2**–**T_4** gradually shifted into a Q^3 absorption peak, as shown in Figure 4. Therefore, with increasing OTES proportion, Si–O replaced Zr–O, and Si–O–Zr was formed. The noise peak reduction indicated that increasing the TEOS proportion enhanced the network structure purity.

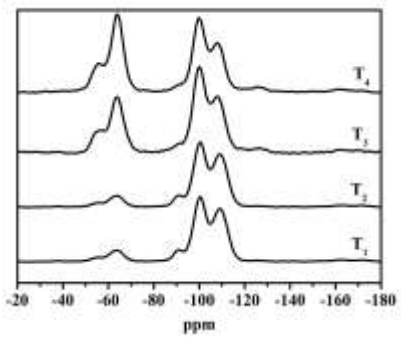

Fig. 4 ^{29}Si-NMR spectra of hybrid material **T_1–T_4**

C. X-Ray diffraction analysis

In this study, we performed an X-ray diffraction analysis of hybrid materials in the **Z**, series with various proportions developed by a sol–gel process. Because neither the series of hybrid materials nor the Zr powder was sintered, all of these materials exhibited amorphous structures without clear crystal phase peaks, as shown in Figures 5. Figure 5 shows that the diffraction peaks of **Z_1**, **Z_2**, **Z_3**, and **Z_4** occur at 2θ = 21.36°, 20.89°, 21.12°, and 21.50°, respectively. These results indicate that with the exception of the Zr powder, the morphology of amorphous-phase OTES and TEOS affected the diffraction peaks of the hybrid materials **Z_1**–**Z_4**.

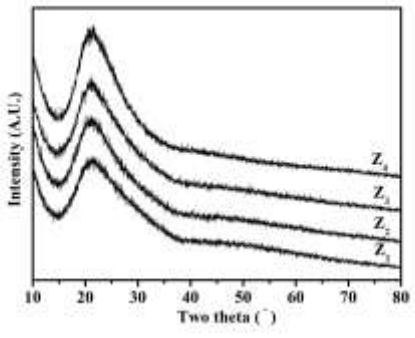

Fig. 5 XRD spectra of **Z_1–Z_4**.

D. Energy-dispersive X-ray spectra analysis

The energy-dispersive X-ray spectroscopy (EDS) analysis results are presented in Table 2 and Figure 6. When additional zirconia gel was added to hybrids **Z_1–Z_4**, the quantity of zirconium increased, which caused the quantity of Si to decrease. It is possible that the carbon proportion decreased and the oxygen increased in the hybrid material because of the formation of additional Zr–O–Zr bonds in zirconia thin films of hybrids **Z_1–Z_4** and the gradually increasing zirconium proportion.

Table 2 shows the results of the EDS analyses of **T_1–T_4**. The molar ratio of the ZNP/TEOS/OTES hybrid material increased with increasing amounts of OTES because the $Si(OH)_3$ structure (formed by hydrolysis–condensation of OTES and TEOS) combined with the zirconia. The Si peaks revealed that the intensity of the ZNP/TEOS/OTES hybrid material increased as the amount of OTES increased. The amounts of carbon and zirconium decreased for the **T_4** hybrid material. This was because the **T_4** ratio formed more Si–O–Si bonds, which is shown by the high Si content in Fig. 6. Furthermore, the amount of zirconium increased in the **Z_4**-treated Cotton fabric. Therefore, a larger hybrid material ratio resulted in greater Zr–O–Si bonding. According to Table 2, when the TEOS and OTES amounts were fixed, the silica content decreased with increasing zirconium content. The maximum **Z_4** via ZNP addition level in the treated cotton fabrics resulted in the maximum zirconium content.

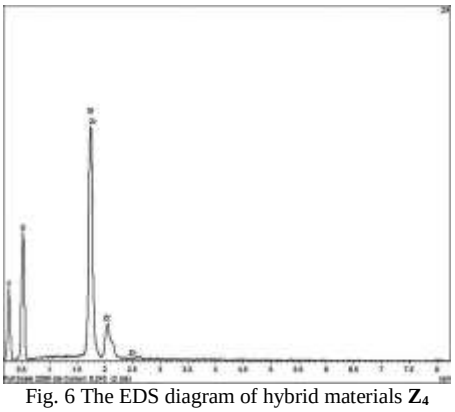

Fig. 6 The EDS diagram of hybrid materials **Z_4**

Table 2: EDS analysis of hybrid materials **Z_1**–**Z_4**, and **T_1**–**T_4**

Samples	Elemental composition (%)			
	C	O	Si	Zr
Z_1	35.5	35.83	24.90	3.77
Z_2	33.23	37.64	24.01	5.12
Z_3	32.51	38.07	22.81	6.61
Z_4	30.31	40.14	22.53	7.02
T_1	35.89	35.54	25.72	2.85
T_2	35.17	35.86	26.4	2.57
T_3	34.23	35.94	26.88	2.95
T_4	34.01	36.25	27.22	2.52

E. Surface morphology of finished cotton fabric

SEM was used to study the morphology of the cotton fabrics. The untreated cotton fabric shows a smooth morphology (Fig. 7a). Figures 7b–7e show SEM images of fabrics treated with varying ZNP molar ratios. An increase in the molar ratio of ZNP with constant amounts of OTES and TEOS revealed irregularly sized particles with a flake-like morphology. As the amount of zirconia increased, the pore size of the treated surface texture decreased as a result of the Zr–O–Zr network structure, which effectively filled the pores of the fabrics, thus improving the water repellency characteristics of the treated fabric. SEM micrographs of fabrics treated with varying OTES molar ratios (Figs. 8a–8d) show irregularly sized particles with a flake-like morphology. Figure 8a shows small particle blocks and uneven distribution of zirconia and silica particles on the surface. As shown in Figs. 8b–8d, the particle distribution was much more uniform with increasing amounts of silica, indicating that the hybrid materials were more evenly dispersed across the fabric, resulting in the formation of a protective layer. Surface-bound particles were more homogeneous in terms of size and distribution and rough regions appeared on the surface. Fabric pores were marginally filled, resulting in a slight increase in the water repellency characteristics and conductivity. Through the above analysis confirms that the Z and T series hybrid materials can be universally processed in cotton dyed fabrics. It also echoes the preamble of using the hydrothermal method to prepare the hybrid materials to uniformly disperse the cotton fabrics and make the surface of materials appear adhesion.

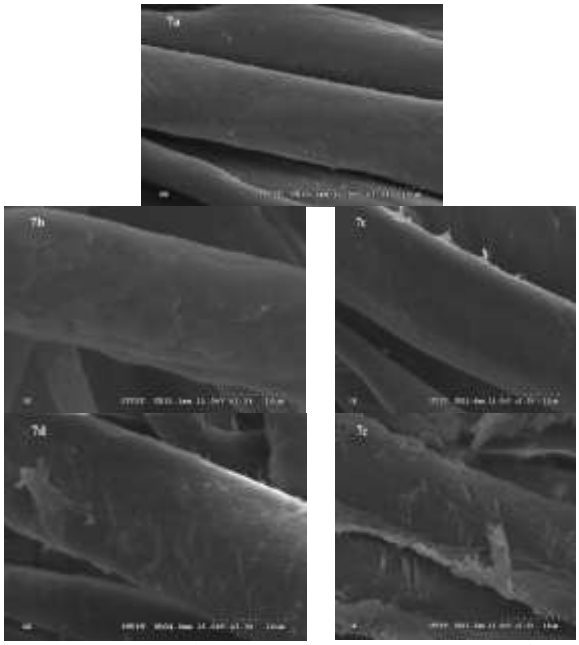

Fig. 7 SEM images of untreated (**C**) and treated (**CZ_1–CZ_4**) fabric (×3000).

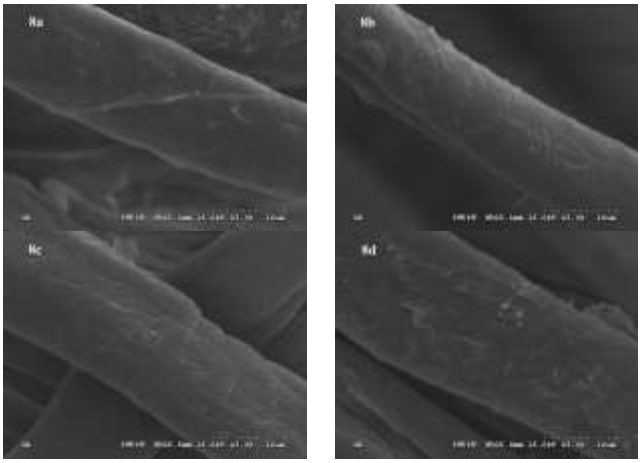

Fig.8 SEM images of **CT_1–CT_4** fabric (×3000).

F. Contact angle analysis of treated cotton fabrics

Table 3 shows the results of the contact angle analysis for the treated cotton fabrics. The contact angle of untreated cotton fabrics was 0°. The average contact angle for **CT_1** before washing was 130.9° and this value increased with increasing OTES molar ratio. The increase of OTES molar ratio, in turn, increased the number of siloxane groups in the hybrid materials, which enhanced crosslinking and improved the water repellency characteristics of the cotton fabrics. Thus, **CT_4** attained the highest contact angle, 138°. The results presented in Figure 9 for the **CZ_1-CZ_4** fabrics show trends similar to those of the **CT_1–CT_4** fabrics as illustrated in Figure 10. However, the contact angles slightly decreased after 10 washing cycles. The reason for these results may be that the hybrid compounds that adhered on the Cotton fabrics were removed from the surface of the fabrics because of mechanical stirring, thereby negatively affecting the contact angle.

By comparing the contact angles of the **CZ_1-CZ_4** fabrics, it can be seen that the fabrics treated with **CZ_4** exhibited the best

Table 3. Surface hydrophobicity evaluation of **CZ_1–CZ_4** and **CT_1–CT_4**.

Compd.	Contact angle (°)		Compd.	Contact angle (°)	
	Before washing	After washing		Before washing	After washing
C	0	0	C	0	0
CZ_1	127.4	120.1	**CT_1**	130.9	123.0
CZ_2	130.1	122.8	**CT_2**	132.0	125.5
CZ_3	132.4	124.0	**CT_3**	135.0	126.7
CZ_4	134.0	126.4	**CT_4**	138.0	131.8

contact angle of 134°. Further, the dyeing showed little effect on the contact angle of the cotton fabrics, as shown in Table 3. The contact angles of **CZ_4** and **CT_4** after washing were 126.4° and 131.8°,

respectively, slightly lower than those of **CZ_4** and **CT_4** before washing.

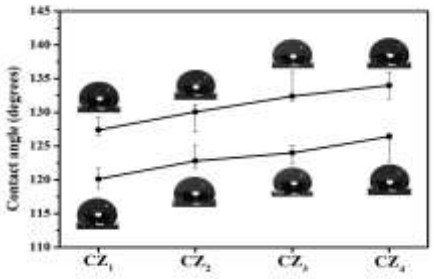

Fig. 9 Contact angle analysis of **CZ_1–CZ_4**.

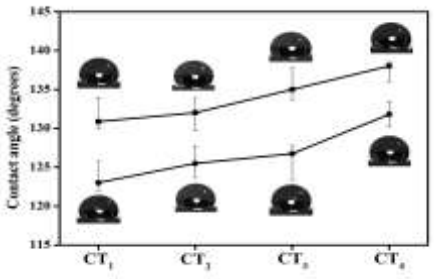

Fig. 10 Contact angle analysis of **CT_1–CT_4**.

G. Warmth retention analysis of processed cotton fabrics CZ_1–CZ_4 and CT_1–CT_4

We used a four-point temperature probe to measure the temperature variation of the finished cloths to determine their thermal insulation properties. The analysis results, shown in Figures 11–12, indicate that the grey cotton cloth exhibited the smallest temperature difference following 600 s of irradiation with a halogen lamp. In the case of the grey finished cloth, **CZ_4**, which had the greatest zirconia sol content, the temperature difference was approximately 31.72 °C, which indicates that the temperature difference increases as the zirconia sol content increases. Thus, the enhanced endothermic effects of the hybrid materials in the finished cloth provided the finished fabric with a thermal storage effect. The insulation properties of the materials improved as the zirconia/ TEOS/OTES sol concentrations were increased. Among finished cloths **CT_1–CT_4**, the largest temperature difference, 28.77 °C, was determined between finished cloth **CT_4** and the cotton grey cloth. Thus, the Z and T series of the finished cloth, with additional TEOS/zirconia sol, exhibited comparatively improved thermal storage capacities. An analysis of the insulation properties of finished cloths **CT_1–CT_4** revealed a temperature difference of 7.35 °C between finished cloth **CT_4** and the cotton grey cloth, which was the optimal result obtained. An analysis of the insulation properties of finished cloths **CZ_1–CZ_4** indicated that there was temperature difference of 8.15 °C between finished cloth **CZ_4** and the polyester grey cloth, which was the optimal result obtained. Therefore, we determined that the zirconia sol alone causes the inorganic zirconium to agglomerate, which reduces the size and number of gaps in the finished cloth and increases the air content. In addition, the properties of the zirconium and agglomerated inorganic zirconium prevented the material from cooling, contributing to the superior thermal insulation properties of the material.

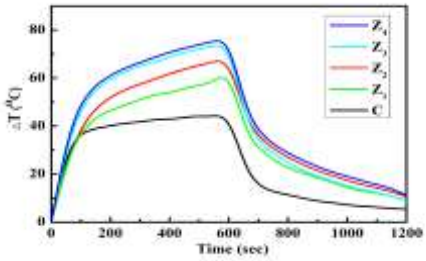

Fig. 11 Warmth retention analysis of **C**, **CZ_1–CZ_4**.

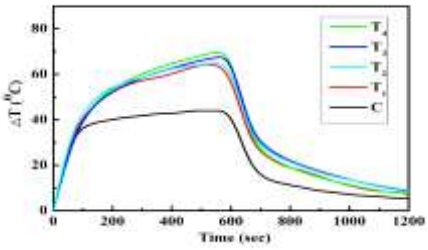

Fig. 12 Warmth retention analysis of **C**, **CT_1–CT_4**.

IV. CONCLUSIONS

Zirconia/silica hybrid materials were synthesized using a hydrothermal process with various molar ratios of the aluminum isopropoxide and OTES chemical precursors. The properties of cotton fabrics coated with the ZNP/TEOS/OTES hybrid materials were examined, and FTIR, ^{29}Si NMR, and EDS analyses confirmed that the zirconia and silica in the hybrid materials bonded to form a network. The FTIR spectra indicated increasing numbers of Si–O–Si and Zr–O–Zr linkages as the molar ratios of ZNP and OTES increased. The diffraction peak of the Zr powder, inoculated Zr-series hybrid material **Z_4** appeared at 2θ = 21.05°. Thus, the addition of adequate amounts of ZNP/TEOS/OTES can improve the water repellency properties of treated cotton fabrics, as indicated by the contact angle results for untreated cotton fabrics (0°) and treated fabrics after washing (120.1–131.8°). The thermal storage analysis indicated that the effects became stronger as the zirconia sol content was increased. There was a temperature difference of 31.72 °C between finished cloth **CZ_4** and the cotton grey cloth. We can infer that the endothermic effects of the zirconia sol in the hybrid materials enhanced the thermal storage capacity of the treated fabrics. The insulation effect that occurred in the case of finished cloth **CZ_4**, in which only zirconia sol was added, resulted in a

temperature increase of 8.15 °C compared with that of the cotton grey cloth.

ACKNOWLEDGMENT

The authors thank the Ministry of Science and Technology of the Republic of China, Taiwan, for financially supporting this research under grant MOST 107-2221-E-168-004. The authors would like to thank Ms. Shu Yi Sun for carrying out Solid State NMR measurements in National Cheng Kung University.

REFERENCES

[1] D. C. Clive, R. Christophe, and J. H. S. Mark, "*Chemical aspects of solution routes to perovskite-phase mixed-metal oxides from metal-organic precursors," Chem. Rev.*, vol. 93, pp. 1205–1241, 1993.

[2] D. A. Loy, and K. J. Shea, "*Bridged polysilsesquioxanes highly porous hybrid organic- inorganic materials*," Chem. Rev., vol. 95(5), pp. 1431–1442, 1995.

[3] J. D. Mackenzie, "*Structures and properties of ormosils*," J. Sol-Gel Sci. Technol., vol. 2(1-3), pp. 81–86, 1994.

[4] F. Hoffmann, M. Cornelius, J. Morell, and M. Fröba, "*Silica-based mesoporous organic–inorganic hybrid*," Angew. Chem. Int. Ed., vol. 45, pp. 3216–3251, 2006.

[5] C. Sanchez, B. Julián, P. Belleville, and M. Popall, "*Applications of hybrid organic–inorganic nanocomposites*," J. Mater. Chem., vol. 15, pp. 3559–3592, 2005.

[6] P. Judeinstein, and C. Sanchez, "*Hybrid organic inorganic materials a land of multidisciplinarity*," J. Mater. Chem., vol. 6(4), pp. 511–525, 1996.

[7] Y. H. Han, A. Taylor, M. D. Mantle, and K. M. Knowles, "*Sol–gel derived organic–inorganic hybrid materials*," J. Non-Cryst. Solids., vol. 353, pp. 313–320, 2007.

[8] R. D. Maggio, S. Dirè, E. Callone, F. Girardi, and G. Kickelbick, "*Hybrid organic–inorganic materials using zirconium based NBBs and vinyl trimethoxysilane: Effect of pre-hydrolysis of silane*," Polymer, vol. 51, pp. 832–841, 2010.

[9] G. Cheng, "*An inorganic–organic hybrid precursor strategy for the synthesis of zirconium diboride powders*," Int. J. Refract. Met. Hard Mater., vol. 36, 149–153, 2013.

[10] J. Zhao, W. Fan, D. Wu, and Y. Sun, "*Synthesis of highly stabilized zirconia sols from zirconium*," J. Non-Cryst. Solids, vol. 261, 15–20, 2000.

[11] K. Joy, S. S. Lakshmy, P. B. Nair, and G. P. Daniel, "*Band gap and superior refractive index tailoring properties in nanocomposite thin film achieved through sol–gel co-deposition method*," J. Alloys Compd., vol. 512, 149–155, 2012.

[12] E. L. Corral and L. S. Walker, "*Improved ablation resistance of C–C composites using zirconium diboride and boron carbide,"* J. Eur. Ceram. Soc., vol. 30, 2357–2364, 2010.

[13] D. R. Clarke and S. R. Phillpot, "*Thermal barrier coatings materials*," Mater. Today, vol. 8(6), 22–29, 2005.

[14] M. Ferraris, E. Verné, P. Appendino, C. Moisescu, A. Krajewski, A. Ravaglioli, and A. Piancastelli, "*Coatings on zirconia for medical appliactions*," Biomaterials, vol. 21, 765–773, 2000.

[15] J. C. S. Wu and L. C. Cheng, "*An improved synthesis of ultrafiltration zirconia membranes via the sol–gel route using alkoxide precursor*," J. Membrane Sci., vol. 167, 253–261, 2000.

[16] P. C. R. Varma, J. Colreavy, J. Cassidy, M. Oubaha, C. McDonagh, and B. Duffy, "*Corrosion protection of AA 2024-T3 aluminium alloys using 3, 4-diaminobenzoic acid chelated zirconium–silane hybrid sol–gels*," Thin Solid Films, vol. 518, 5753–5761, 2010.

[17] P. Shojaee and A. Afshar, "*Corrosion effects of zirconia content on characteristics and corrosion behavior of hydroxyapatite ZrO2 biocomposite coatings codeposited by electrodeposition*," Surf. Coat. Technol., vol. 262, 166–172, 2015.

[18] P. K. Q. Nguyen and S. K. Lunsford, "*Electrochemical response of carbon paste electrode modified with mixture of titanium dioxide zirconium dioxide in the detection of heavy metals: Lead and cadmium*," Talanta, vol. 101, 110–121, 2012.

[19] M. Răileanu, L. Todan, M. Voicescu, N. Drăgan, D. Crişan, M. Maganu, D. M. Vuluga, A. Ianculescu, D. C. Culiţă, "*Sol-gel zirconia-based nanopowders with potential applications for sensors,"* Ceram. Int., vol. 41, 4381–4390, 2015.

[20] S. Jesurani, S. Kanagesan, M. Hashim, and I. Ismail, "*Dielectric properties of Zr doped CaCu3Ti4O12 synthesized by sol–gel route*," J. Alloys Compd., vol. 551, 456–462, 2013.

[21] J. Dong, Y. Wen, Y. Miao, Z. Xie, Z. Zhang, and H. Yang, "*A nanoporous zirconium phytate film for immobilization of redox protein and the direct electrochemical biosensor*," Sens. Actuators, B, vol. 150, 141–147, 2010.

[22] B. Lu and Y.S. Lin, "*Sol–gel synthesis and characterization of mesoporous yttria-stabilized zirconia membranes with graded pore structure*," J. Mater. Sci., vol. 46, 7056–7066, 2011.

[23] M. Kumar and G.B. Reddy, "*Effect of sol-age on the surface and optical properties of sol-gel derived mesoporous zirconia thin films*," AIP Adv., vol. 1, 22111(1–10), 2011.

[24] Z. Wen, E.M. James, R.U. Marilyn and E.A. Fred, "*Toughening of a high-temperature polymer by the sol–gel, in situ generation of a rubbery silica–siloxane phase*," J. Appl. Polym. Sci., vol. 79, 2326–2330, 2001.

[25] C. Anderson and A.J. Bard. "*An improved photocatalyst of TiO2/SiO2 prepared by a sol-gel Synthesis*," J. Phys. Chem., vol. 99, 9882–9885, 1995.

[26] O. Kesmez, H.E. Camurlu, E. Burunkaya and E. Arpac, "*Sol–gel preparation and characterization of anti-reflective and self-cleaning SiO2–TiO2 double-layer nanometric films*," Sol. Energ. Mat. Sol. C., vol. 93, 1833–1839, 2009.

[27] M. Houmard, D. Riassetto, F. Riassetto, A. Bourgeois, G. Berthome, J. C. Joud and M. Langlet, "*Morphology and natural wettability properties of sol–gel derived TiO2–SiO2 composite thin films*," Appl. Surf. Sci., vol. 254, 1405–1414, 2007.

[28] S.J. Khatib and S.T. Oyama, "*Silica membranes for hydrogen separation prepared by CVD,"* Sep. Purif. Technol., vol. 111, 20–42, 2013.

[29] J. Zhu, B. Y. Tay and J. Ma, "*Hydrothermal synthesis and characterization of mesoporous SnO2–SiO2,"* J. Mater. Process. Tech., vol. 192–193, 561–566, 2007.

[30] K. Byrappa, A.K. Subramani, S. Ananda, K.M.L. Rai, M.H. Sunitha, B. Basavalingu and K. Soga, "*Impregnation of ZnO onto activated carbon under hydrothermal conditions and its photocatalytic properties,*" J. Mater. Sci., vol. 41, 1355–1362, 2006.

[31] S.Y. Wu, W. Zhang and X.M. Chen, "*Formation mechanism of NaNbO3 powders during hydrothermal synthesis*," J. Mater. Sci. Mater. El., vol. 21, 450–455, 2010.

[32] Z. Hui, L. Fang and Z. Hong, "*Immobilization of TiO2 nanoparticles on PET fabric modified with silane coupling agent by low temperature hydrothermal method*," Fiber. polym., vol. 14(1), 43–51, 2013.

[33] J. Choi, S. Komarneni, K. Grover, H. Katsuki and M. Park, "*Hydrothermal synthesis of Mn–mica,"* Appl. Clay Sci., vol. 46, 69–72, 2009.

[34] R. Pazik, D. Hreniak and W. Strek, "*Microwave driven hydrothermal synthesis of Ba1−xSrxTiO3 nanoparticles*," Mater. Res. Bull., vol. 42, 1188–1194, 2007.

[35] Y.Q. Wang, J.F. Huang Z.H. Chen and L.Y. Cao, "*Preparation and phase composition optimization of yttrium silicates SiC multilayer coating coated carbon carbon composites*," J. Compos. Mater., vol. 46(4), 409–415, 2011.

[36] X. Wu, B. Zhang and Z. Hu, "*Microwave hydrothermal synthesis of boehmite hollow microspheres*," *Mater. Lett.*, vol. 73, 169–171, 2012.

[37] Rajib Saha, Md. Jahidul Islam, Mahade Hasan Ikram, Asha Akter Ete. "A comparative study on acidic and neutral enzyme on various properties before and after reactive dyeing" International Journal of Engineering Trends and Technology 67.11 (2019)